Active molecular iodine photochemistry in the Arctic

Angela R. W. Raso[a,b], Kyle D. Custard[a], Nathaniel W. May[b], David Tanner[c], Matt K. Newburn[d], Lawrence Walker[d], Ronald J. Moore[d], L. G. Huey[c], Liz Alexander[d], Paul B. Shepson[a,e,f], and Kerri A. Pratt[b,g,1]

[a]Department of Chemistry, Purdue University, West Lafayette, IN 47907; [b]Department of Chemistry, University of Michigan, Ann Arbor, MI 48109; [c]School of Earth and Atmospheric Sciences, Georgia Institute of Technology, Atlanta, GA 30332; [d]Environmental Molecular Sciences Laboratory, Pacific Northwest National Laboratory, Richland, WA 99352; [e]Department of Earth, Atmospheric, and Planetary Sciences, Purdue University, West Lafayette, IN 47907; [f]Purdue Climate Change Research Center, Purdue University, West Lafayette, IN 47907; and [g]Department of Earth & Environmental Sciences, University of Michigan, Ann Arbor, MI 48109

Edited by Mark H. Thiemens, University of California, San Diego, La Jolla, CA, and approved August 15, 2017 (received for review February 17, 2017)

During springtime, the Arctic atmospheric boundary layer undergoes frequent rapid depletions in ozone and gaseous elemental mercury due to reactions with halogen atoms, influencing atmospheric composition and pollutant fate. Although bromine chemistry has been shown to initiate ozone depletion events, and it has long been hypothesized that iodine chemistry may contribute, no previous measurements of molecular iodine (I_2) have been reported in the Arctic. Iodine chemistry also contributes to atmospheric new particle formation and therefore cloud properties and radiative forcing. Here we present Arctic atmospheric I_2 and snowpack iodide (I^-) measurements, which were conducted near Utqiaġvik, AK, in February 2014. Using chemical ionization mass spectrometry, I_2 was observed in the atmosphere at mole ratios of 0.3–1.0 ppt, and in the snowpack interstitial air at mole ratios up to 22 ppt under natural sunlit conditions and up to 35 ppt when the snowpack surface was artificially irradiated, suggesting a photochemical production mechanism. Further, snow meltwater I^- measurements showed enrichments of up to ∼1,900 times above the seawater ratio of I^-/Na^+, consistent with iodine activation and recycling. Modeling shows that observed I_2 levels are able to significantly increase ozone depletion rates, while also producing iodine monoxide (IO) at levels recently observed in the Arctic. These results emphasize the significance of iodine chemistry and the role of snowpack photochemistry in Arctic atmospheric composition, and imply that I_2 is likely a dominant source of iodine atoms in the Arctic.

atmosphere | iodine | cryosphere | snowpack | photochemistry

Atmospheric boundary layer ozone depletion events (ODEs), during which ozone (O_3) in the lower troposphere rapidly drops from background levels of 30–40 ppb to below 10 ppb, have been observed during springtime in the polar regions for several decades (1, 2). Early measurements of filterable halogens (bromine, chlorine, and iodine) (3) showed a particularly strong correlation between filterable bromine and O_3 concentrations, suggesting the catalytic destruction of O_3 by bromine atoms (4). Subsequent observations of inorganic bromine (Br_2, BrO, HOBr) in the polar regions (5–10) have elucidated the "bromine explosion" chemical mechanism (11, 12). Still, modeling studies suggest that this system is far from fully understood, and bromine chemistry alone cannot explain the full extent of ODEs that occur (13–16). The presence of iodine compounds, even at small mole ratios (moles of analyte/mole of air), may significantly increase the rate of O_3 destruction during ODEs (13, 17, 18), due to the relatively large rate constant for the reaction of BrO with IO [$k = 9.4 \times 10^{-11}$ $cm^3 \cdot molecule^{-1} \cdot s^{-1}$ (19)] compared with the BrO self-reaction [$k = 9.3 \times 10^{-13}$ $cm^3 \cdot molecule^{-1} \cdot s^{-1}$ (20)] (R31, 33; Fig. 1). Recently, inorganic chlorine (Cl_2, ClO) (21, 22) and iodine (IO, HIO_3) (23, 24) have been observed in the Arctic, adding support to signs of the importance of iodine chemistry from early aerosol measurements (3). Although molecular iodine (I_2) has not previously been observed in the Arctic, it has been observed at several midlatitude marine and coastal sites (25) and along the Antarctic coast (26), and IO has been observed in the Antarctic (16, 27, 28), and in the sub-Arctic (29). During recent measurements at Alert, Canada, IO was observed at levels up to 1.5 ppt (23). Iodine has recently been observed to contribute to atmospheric new particle formation (30) through the sequential addition of iodic acid (HIO_3) at maximum Arctic mole ratios of ∼1 ppt (24), giving further evidence to the presence and importance of Arctic iodine chemistry.

Although there is a clear indication of iodine chemistry in the Arctic, the source of the inorganic iodine has not been clear. In most midlatitude observations of I_2 and IO, the source of inorganic iodine is believed to be macroalgae under oxidative stress, such as during low tide (31–33). In the Antarctic, observations have previously been ascribed to I_2 production by sea ice diatoms, which are commonly found on the underside of both Arctic and Antarctic sea ice, followed by I_2 diffusion through open brine channels to the sea ice surface (25, 34, 35). However, although the diffusion of I_2 through brine channels has been modeled (34), it has not been directly observed. Whether iodine precursors in the Arctic are emitted from the open ocean (23, 29) or from sea ice-covered regions (24) has remained unclear. There are potential mechanistic pathways for both sources. Br_2, Cl_2, and BrCl production via photochemical reactions has been demonstrated in the Arctic saline snowpack (7, 9, 36) and from frozen substrates in laboratory experiments (37–44). I_2 and triiodide (I_3^-) have recently been shown to be photochemically produced in Antarctic snow spiked with iodide (1–1,000 μM) (45), and iodate (IO_3^-) has also been shown to be photochemically active in frozen solutions (46). These studies show condensed phase iodine photochemistry, and although previous samples have lacked the physical and chemical characteristics of authentic snow, they suggest that photochemical production of I_2, similar to that of Br_2, Cl_2, and BrCl production in the Arctic surface snowpack (7, 36), is probable. However, neither atmospheric I_2 nor the production of I_2 from snow samples with natural iodide (I^-) levels has ever been reported.

Significance

We report here the first measurements of molecular iodine (I_2) in the Arctic atmosphere and iodide (I^-) in the Arctic snowpack. Although iodine chemistry is expected to have significant impacts on Arctic atmospheric ozone destruction and new particle production, sparse measurements of atmospheric iodine have limited our ability to examine sources and impacts. We show, through sunlit and artificially irradiated snowpack experiments, that the coastal Arctic snowpack is capable of photochemical production and release of I_2 to the boundary layer. This is supported by enrichment of the snowpack in I^- compared with that expected from sea spray influence alone. Through photochemical modeling, we demonstrate that, at observed I_2 levels, snowpack production can have a significant impact on Arctic atmospheric chemistry.

Author contributions: A.R.W.R., K.D.C., P.B.S., and K.A.P. designed research; A.R.W.R., K.D.C., N.W.M., M.K.N., L.W., R.J.M., L.A., and K.A.P. performed measurements; D.T. and L.G.H. contributed new analytic tools; A.R.W.R., N.W.M., and K.A.P. analyzed data; and A.R.W.R. and K.A.P. wrote the paper.

The authors declare no conflict of interest.

This article is a PNAS Direct Submission.

[1]To whom correspondence should be addressed. Email: prattka@umich.edu.

This article contains supporting information online at www.pnas.org/lookup/suppl/doi:10.1073/pnas.1702803114/-/DCSupplemental.

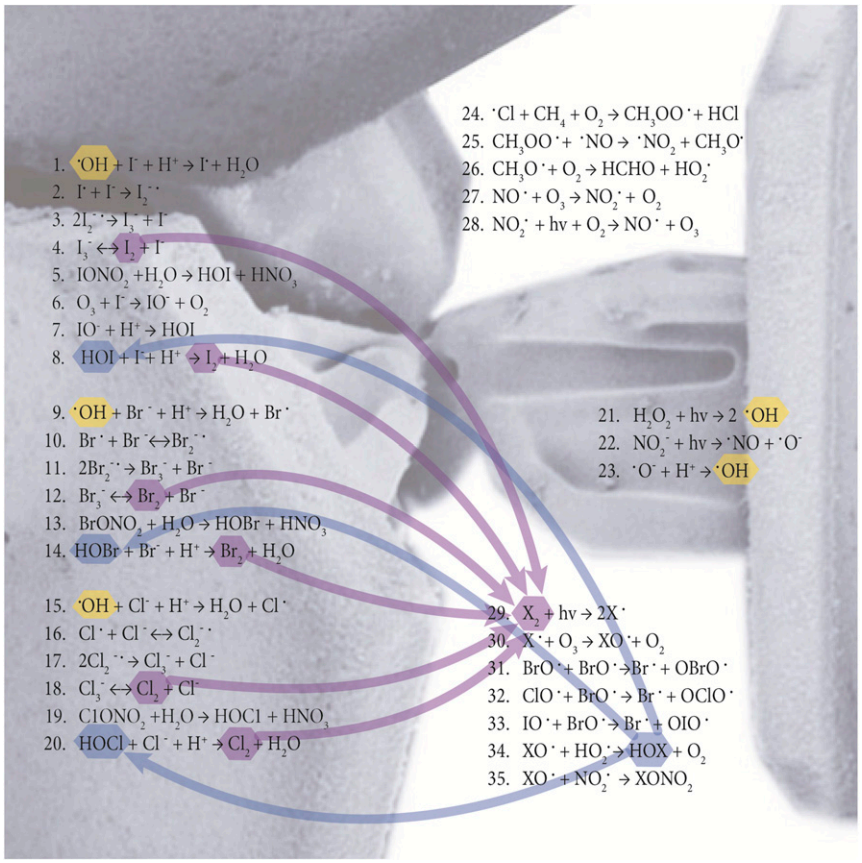

Fig. 1. Snowpack halogen production and interstitial air halogen reactions. Major halogen reactions proposed to occur in the interstitial snowpack air and within the snow surface are shown. Oxidation of I^- in the dark (R6–R8) is based on Carpenter et al. (47). Photochemical oxidation of Br^- (R9–R12) is based on Abbatt et al. (38). Cl^- and I^- photochemical oxidation reactions (R15–R18 and R1–R4, respectively) are suggested to be analogous. Snow crystal SEM image is an open source image from the Electron and Confocal Microscopy Laboratory, Agricultural Research Service, US Department of Agriculture.

Given the expected importance of iodine chemistry in the atmosphere (24, 25), snowpack iodine chemistry was investigated near Utqiaġvik, AK, in February 2014. Here, we report Arctic I_2 measurements, in both the tropospheric boundary layer and snowpack interstitial air, coupled with measurements of I^- in Arctic snow. The effect of radiation on halogen mole ratios in the snowpack interstitial air was examined through sunlit experiments, artificial irradiation experiments, and snowpack vertical profiles. In addition, the sensitivity of ozone depletion rates and IO mole ratios to tropospheric I_2 was examined using a zero-dimensional photochemical model.

Results and Discussion

Snowpack Molecular Iodine Production. Here we report observations of I_2 and snowpack I^- in the Arctic. Gas-phase I_2 was observed in the snowpack interstitial air at 10 cm below the sunlit snowpack surface on February 1 and 2, 2014, near Utqiaġvik, AK (Fig. 2). I_2 mole ratios in the snowpack interstitial air peaked at 2.7–5.1 ppt in the early afternoon, just following the solar radiation maxima (Fig. 2). Coincident with these daytime maxima, I_2 was observed in the boundary layer, 1 m above the snowpack surface, at mole ratios of ∼0.3–1.0 ppt (Fig. 2). Significantly more I_2 was observed in the snowpack interstitial air on February 2 (maximum I_2 5.1 ppt), which was sunny and clear (maximum radiation 172 W/m^2), compared with February 1 (maximum I_2 2.7 ppt), which was overcast (maximum radiation 18 W/m^2), further supporting a photochemical production mechanism. Laboratory studies have shown that I_2 can be produced from aqueous samples containing I^- in the presence of O_3 without light, via reactions 6–8 (Fig. 1) (47). During the night of February 1–2, average wind speeds rose from 2.0 m·s^{-1} to 5.9 m·s^{-1}, leading to increased wind pumping, resulting in increasing O_3 from 5 to 25 ppb in the snowpack interstitial air over the course of ∼30 min [22:00–22:30 Alaska Standard Time (AKST)] (Fig. 2). This presents an opportunity to examine the influence of O_3 on dark oxidation and subsequent I_2 formation. However, although an apparent small increase in I_2 signal at a snowpack depth of 10 cm was observed during this time (Fig. 2), the I_2 levels were never statistically significant different from zero. Therefore, these observations suggest that snowpack photochemical reactions were the predominant source of the observed I_2 in the Arctic boundary layer.

The photochemical nature of I_2 production in the snowpack is further demonstrated by the differences in the vertical profiles of I_2 and molecular bromine (Br_2) within the snowpack interstitial air (Fig. 3). Gas-phase I_2 and Br_2 were simultaneously quantified at mole ratios up to 22 and 43 ppt, respectively, under sunlit conditions in the snowpack interstitial air, as shown in Fig. 3. Br_2 showed peak mole ratios (43 ppt) just below the snowpack/atmosphere interface (within the top ∼10 cm) (Fig. 3 and Fig. S1). This is consistent with previous measurements, which showed a maximum in Br_2 mole ratios within the top 7 cm of the snowpack air at Alert, Canada (9). In contrast, the I_2 peak mole ratio (22 ppt) was observed at ∼40 cm below the snowpack surface, at least 30 cm deeper than the Br_2 maximum (Fig. 3). At this snow depth, ambient light was attenuated (at 40 cm, ∼2% of 400 nm light remains) (48). The difference in behavior between I_2 and Br_2 with depth reflects two factors. First, I_2 photolyzes nearly four times faster than Br_2 (I_2 $J_{max} = 2.9 \times 10^{-3}$ s^{-1} vs. Br_2 $J_{max} = 8.6 \times 10^{-4}$ s^{-1} for above the snowpack on February 2, 2014). Second, whereas bromide (Br^-) shows no consistent enrichment (relative to the seawater Br^-/Na^+ ratio) with depth (Fig. S2), I^- was increasingly enriched with depth in January and February 2014 snow meltwater (Fig. 3). I^- was observed at concentrations of 1.4–4.3 nM (Fig. S2) that are greatly enriched relative to sodium (Na^+), at up to ∼1,900 times the seawater ratio (I^-/Na^+) (Fig. 3). The I^- concentrations in the surface snowpack (top 7 cm) meltwater (2.0 ± 0.6 nM; Fig. S2) were sufficient to produce ∼1,600 ppt of I_2, if I^- were completely converted to I_2 and contained in the snowpack interstitial air (*SI Methods*). In comparison, snow meltwater Br^- ranged from partially depleted to double that in

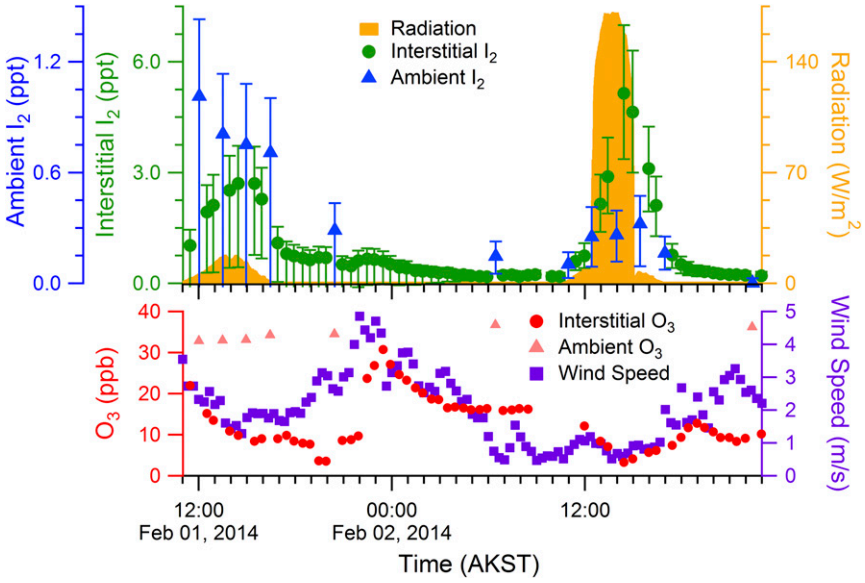

Fig. 2. I_2, O_3, radiation, and wind speeds during February 1–2, 2014. The diurnal profiles for I_2 and O_3 mole ratios, as well as the radiation and wind speeds, are shown as 20-min averages from February 1 to 2, 2014. Error bars are propagated uncertainties (*SI Methods*). Ambient measurements were conducted 1 m above the snowpack surface. Interstitial air measurements were conducted 10 cm below the snowpack surface. Fluctuations in interstitial air O_3 mole ratios correlate with high wind speeds and are therefore likely due to wind pumping.

seawater (0.58–2.0 times the seawater Br^-/Na^+ ratio; Fig. S2). Previous measurements of Br^-/Na^+ ratios in coastal surface snow have shown bromide enrichments, relative to seawater, to increase from late winter (1.5–5 times the seawater Br^-/Na^+ ratio) through early spring (20–72 times the Br^-/Na^+ ratio in seawater), which is consistent with active heterogeneous recycling of bromine on the snowpack (49, 50). The much greater snowpack enrichment factor for I^- suggests production and transport of iodine compounds from upwind snowpack; ocean or saline sea ice environments; or aerosols, and subsequent deposition on the downwind coastal snowpack. The exact source of I^- to the snowpack remains undetermined, but the increasing enrichment of I^- with depth indicates that iodine near the surface has migrated, either redepositing deeper in snowpack and/or being lost from the snowpack surface to the atmosphere, perhaps following polar sunrise. Although the source of I^- enrichment in the Arctic snowpack requires further investigation, deposition of gas or particle phase iodine is consistent with earlier findings of enriched iodine in the aerosol phase (3). Future measurements of the spatial and temporal heterogeneity of snowpack I^- enrichment are needed to elucidate the migration of iodine in the Arctic system.

To further investigate photochemical I_2 production, the snowpack was exposed to artificial UV light (Fig. 4). This experiment was conducted during the night and morning when solar radiation was low (<20 W/m^2). When exposed to artificial light, the snowpack rapidly produced up to 35 ppt of gas-phase I_2 at a depth of 10 cm (Fig. 4). The radiation spectrum of the lights used (Fig. S3) is adequate for the photolytic production of hydroxyl radicals from hydrogen peroxide and nitrite (Fig. 1, R21–R23), but not for significant I_2 photolysis, which occurs most efficiently at wavelengths greater than 400 nm (20, 51). Upon snow illumination, Br_2 was also quickly produced in the snowpack interstitial air, yielding mole ratios of 40–80 ppt (Fig. 4). With halogen production in the snowpack, O_3 decayed rapidly, via the chemistry shown in Fig. 1. When the lights were turned off, both Br_2 and I_2 mole ratios decayed, and O_3 partially recovered. This molecular halogen decline was likely controlled by dilution with ambient air (wind pumping), a lack of photochemical halogen production, and adsorption/desorption of halogen species onto the snow. Although snow grain chemical composition and exchange processes are complex (52), the rate of desorption from aqueous surfaces is often described as inversely proportional to the Henry's Law constant for that species (53). Because I_2 is more soluble (k_H = 41.9 M/atm at −20 °C) than Br_2 (k_H = 8.4 M/atm at −20 °C) (54), its rate of desorption from the disordered snow interface is expected to be slower, as shown in Fig. 4 by the slower decay in I_2 mole ratios after illumination ceases, and from the slower initial rise in I_2 mole ratios upon illumination. I_2 and Br_2 were again observed upon snowpack reillumination (Fig. 4). This demonstrates that I_2 and Br_2 are both characterized by condensed-phase photochemical production mechanisms.

The I_2 multiphase photochemical production mechanism proposed here (Fig. 1) is analogous to that for Br_2 production, which occurs first by condensed-phase photochemistry and then is greatly enhanced by gas-phase recycling of Br atoms in the presence of O_3 (7, 37). The suggested mechanism for I_2 production begins in the disordered interface of the aqueous phase on the snow grain surface (52) with oxidation of I^- to an iodide radical by a photochemically produced oxidant (R1), likely the hydroxyl radical, produced by nitrite photolysis in Utqiaġvik snow (R22–R23)

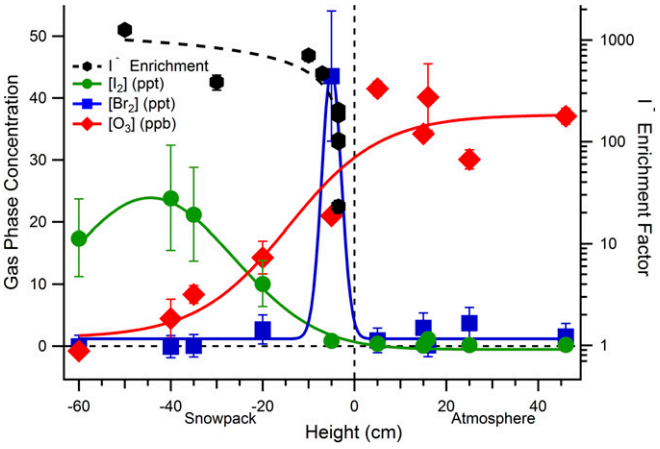

Fig. 3. Vertical profiles of near-surface atmospheric and snowpack interstitial air I_2, Br_2, and O_3 mole ratios, as well as snow I^- enrichment. Gas-phase measurements were made during daylight from 12:22 to 16:23 AKST on February 4, 2014, at heights above (positive) and below (negative) the snowpack surface. Error bars for species measured with CIMS (I_2 and Br_2) are propagated uncertainties (*SI Methods*). Error bars on the O_3 measurements are the SDs of 9- to 22-min averages at each height. I^- enrichment factors (the ratio of I^- to Na^+ in snow meltwater relative to the same ratio in seawater) are shown for snow samples collected from January 27 to February 5, 2014. I^- enrichment factor error bars are the propagated error from three measurements of the I^- concentration in a single sample. See Fig. S1 for an additional set of vertical profile measurements from February 3, 2014.

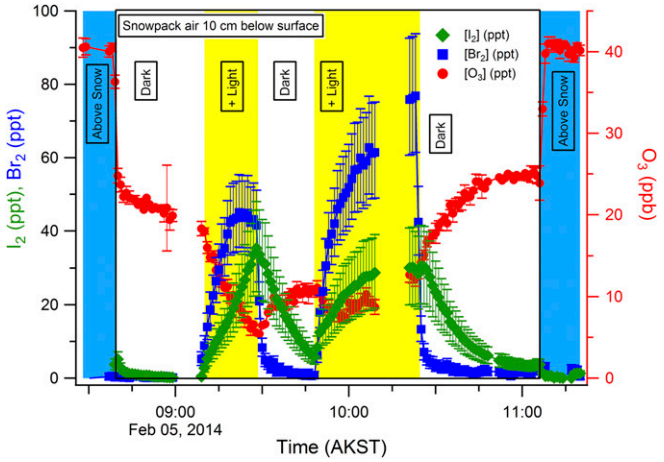

Fig. 4. Snowpack artificial irradiation experiment. Snowpack interstitial air Br_2, I_2, and O_3 mole ratios are shown as 1-min averages for dark and artificial light measurement periods during an experiment on February 5, 2014. Error bars for I_2 and Br_2 are propagated uncertainties (*SI Methods*). The interstitial air measurements were bracketed by near-surface (5 cm above the snowpack surface) measurements of boundary-layer air. The duration of the experiment occurred before the sun rose, allowing for near-complete darkness when the artificial lights were off.

(55). The iodide radical then further reacts in solution to form I_3^- (R2–R3), which has been recently observed in snow samples spiked with I^- (45). I_3^- then decomposes, forming I_2 (R4). I_2 can then be released from the condensed phase to the gas phase, where it rapidly photolyzes in the presence of sunlight. The resulting iodine atoms react with O_3 to form IO (R30). IO can then react with HO_2 to form HOI (R34) or NO_2 to form $IONO_2$ (R35), which can each then be redeposited onto the snow grain surface to reproduce I_2 in a catalytic cycle similar to the bromine explosion (56). Interhalogen reactions may also participate in the production of molecular halogens. HOBr has also been shown to oxidize Cl^- on frozen surfaces to form BrCl when the Br^-/Cl^- ratio is low (37, 39, 40). Similarly, HOI and $IONO_2$ can react on frozen surfaces with Br^- and Cl^- to form IBr and ICl (57). The production of IBr via the reaction of HOI and Br^- is up to ~200 times faster ($k = 3.3 \times 10^{12}$ $M^{-2}{\cdot}s^{-1}$) (58) than the production of Br_2 via the reaction of HOBr and Br^- ($k = 1.6 \times 10^{10}$ $M^{-2}{\cdot}s^{-1}$) (59). Although the interactions between halogen species in the gas phase have received some study, the condensed-phase interactions of halogens have been significantly understudied (56).

Simulations of Arctic Ozone Destruction. Because even small levels of I_2 can significantly impact Arctic atmospheric chemistry, a zero-dimensional photochemical model was used to simulate O_3 depletion and IO production. Because an ODE was not observed during the January to February 2014 study [ODEs typically begin in March in Utqiaġvik (2)], previous observations of atmospheric Br_2, Cl_2, and HOBr from the same location on March 11, 2012 were used to constrain the model (Fig. S4). On this day, atmospheric O_3 decreased from ~20 ppb to <1 ppb over the course of 7 h (Fig. 5*A*), with winds blowing from north to northeast over the consolidated snow-covered ice on the Beaufort Sea. The overall observed ozone depletion rate (3.0 ppb·h^{-1} over the 7-h period) is typical of a large number of ODEs observed over the snow-covered sea ice on the Arctic Ocean (average of 3.5 ppb·h^{-1}) (60). The initial depletion (from 14:00–16:10 AKST) occurred at a rate of 2.2 ppb·h^{-1} and was interrupted by a local atmospheric mixing event (16:10–18:00 AKST), which is not possible to simulate with a zero-dimensional model.

Given that I_2 was only measured in early February in this study, it is plausible that higher mole ratios are present in March, when ODEs regularly occur. Therefore, the model was used to test the sensitivity of O_3 depletion rates to I_2 mole ratios from 0–2.4 ppt (Fig. 5*A*). Without the inclusion of iodine chemistry, O_3 was simulated to deplete initially (14:00–16:10 AKST) at a rate of 1.3 ppb·h^{-1} (Fig. 5*A*), mostly from bromine atom chemistry. However, as shown in Fig. 5*A*, the addition of 0.3 ppt of I_2 (as observed on February 2, 2014) increases the initial rate of ozone depletion by 31%, to 1.7 ppb·h^{-1}. The best fit to the observed initial ozone depletion rate (2.2 ppb·h^{-1}) corresponds to the inclusion of 0.6 ppt of I_2 (within the range of our observations), which causes the model to simulate the initial depletion at a rate of at 2.1 ppb·h^{-1}. The significant increase in the simulated ozone depletion rate with the inclusion of only 0.6 ppt I_2 demonstrates the importance of even a small amount of iodine on the depletion of boundary layer O_3. Higher, but still very modest and plausible, I_2 mole ratios (compared with the ~18 ppt of Br_2 present) have a pronounced effect on the predicted O_3. The addition of 2.4 ppt of I_2 triples the rate of O_3 depletion for the initial period (14:00–16:10 AKST) to 4.0 ppb·h^{-1}.

The sensitivity of simulated IO concentrations to varying amounts of I_2 on March 11, 2012 was also examined (Fig. 5*B*). The simulation containing 2.4 ppt of I_2 produced a maximum of 1.6 ppt of IO, which is near the highest mole ratios observed (1.5 ppt) in Alert, Canada (23). The simulation with 0.3 ppt of I_2 (February 2, 2014, maximum mole ratio) revealed IO mole ratios similar to those most commonly observed at Alert (~0.3 ppt) (23). It should be noted, however, that there are significant uncertainties associated with modeling gas-phase iodine chemistry. Variations in the branching ratio for the products of the reaction of IO with itself can significantly change predicted IO mole ratios. The branching ratios used here (38% I + OIO, 16% I + I, 46% IOOI) may cause overestimation of IO by up to ~10% (61). Additionally, because the photolysis of higher-order iodine oxides (I_2O_3 and larger) could cause the simulated O_3 ratios shown here to be overestimated by up to 18% (17), sub-parts per trillion levels of I_2 may result in even greater ozone depletion rates than predicted here. Even with these uncertainties in simulating iodine chemistry, our snowpack and ambient I_2 observations along

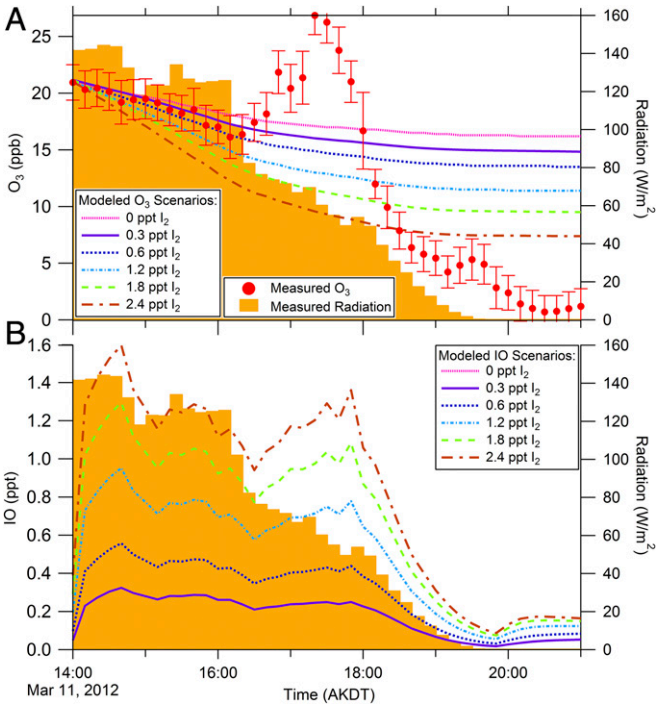

Fig. 5. Model results show the influence of I_2 on (*A*) tropospheric ozone depletion rates and (*B*) IO mole ratios. An ozone depletion event occurring on March 11, 2012 was simulated with I_2 mole ratios between 0 and 2.4 ppt. Cl_2, Br_2, and HOBr were constrained to measurements as shown in Fig. S4. (*A*) Measured O_3 with SDs of the 10-min average, and model results showing simulated O_3 mole ratios. (*B*) Simulated IO mole ratios during the same period.

with our model results demonstrate that even a small amount of I_2, at the observed levels, can significantly increase O_3 depletion rates, while also producing realistic IO mole ratios.

Conclusions

Here we report measurements of I_2 in the Arctic. Low mole ratios (0.3–1.0 ppt) of I_2 in the boundary layer air coupled with elevated I_2 mole ratios in the snowpack interstitial air suggest that the snowpack is a source of I_2 to the Arctic boundary layer. These results are supported by Arctic snowpack measurements of I^-, which was greatly enriched relative to seawater, and more so with increasing depth. I_2 is observed in the snowpack interstitial air under naturally sunlit conditions, and under artificial irradiation, but not in the dark, suggesting a photochemical production mechanism. The inclusion of observed molar ratios of I_2 in a zero-dimensional model increases the ability of the model to simulate the initial rate of an observed ozone depletion event, and produces IO concentrations consistent with recent observations. Differences in the snowpack depth profiles of bromine and iodine species within both the snow phase (Br^- and I^-) and snowpack interstitial air (Br_2 and I_2) suggest that there are significant differences in bromine and iodine multiphase chemistry. The assumption that these species act similarly may be an oversimplification—one that can only be remedied through further measurements of production examining important chemical mechanisms and fundamental reaction rates and yields under both laboratory and field conditions.

The community's challenge to properly simulate the chemical and physical processes that occur within and on the surface of snow grains (62) is especially daunting, because we do not currently understand the physical nature of the phase in which the chemistry is occurring (52, 62). New methodology is required to examine the chemical composition of ambient snow grain surfaces in situ. Although we lack comprehensive knowledge about the heterogeneous chemical processes of halogens on snow, we benefit greatly from real-world observations, such as those described herein. Multiphase interhalogen chemistry may also be important; however, there are no reported ambient measurements of the iodine molecular interhalogens (IBr and ICl). It is also unclear how the likely increasingly saline surface snowpack (from increasing first-year sea ice, sea spray production, and potentially decreasing snow depth), combined with increasing Arctic development (which may be changing acid deposition), are influencing springtime halogen chemistry. Iodine chemistry may have an especially large impact on atmospheric composition as the Arctic warms, given the prevalence of iodine chemistry in the marine midlatitudes (25).

Even at sub-parts per trillion levels of I_2 in the Arctic atmosphere, iodine chemistry has significant impacts on atmospheric boundary layer oxidation capacity and composition, impacting pollutant fate and particle formation. Further simultaneous measurements of aerosol I^-, snowpack I^-, and I_2 are needed to examine the movement of iodine between the aerosol, gas, and the snowpack phases. We now know that the coastal Arctic snowpack is a source of photochemically reactive inorganic iodine. This provides an abiotic source of iodine for new particle formation, expanding the potential importance of this chemical process to impacts on clouds (24, 25, 63). Given the dramatic impact of iodine on Arctic atmospheric composition, there is a need for further measurements of I_2 in the ambient atmosphere to connect and elucidate the full cycling of iodine in the Arctic system.

Methods

Trace halogen gases were measured using chemical ionization mass spectrometry (CIMS), as described by Liao et al. (5, 64), Peterson et al. (8), and Custard et al. (22), on the Barrow Environmental Observatory (BEO), 5 km inland over tundra snowpack near Utqiaġvik, AK, on March 11, 2012, and February 1–5, 2014. A detailed description of the sampling, calibrations, background measurements, line loss tests, and uncertainties are described in *SI Methods*. Briefly, in 2012, CIMS, using IH_2O^- as the reagent ion, measured Br_2, Cl_2, and HOBr at ∼1 m above the snowpack surface [Peterson et al. (8), Custard et al. (22); *SI Methods*]. For 2014 measurements, the CIMS instrument was modified by the addition of an 18-cm-long PTFE-coated flow tube to the original 4.5-cm flow tube. CIMS measurements in 2014 were made using SF_6^- as the reagent ion; masses 254 amu ($^{127}I_2^-$), 160 amu ($^{81}Br^{79}Br^-$), and 158 amu ($^{79}Br_2^-$) were monitored. Calibrations were performed using I_2 and Br_2 permeation devices (VICI) every 30 min to 2 h. Background measurements were performed every 20 min to 1 h, for 7–20 min, by passing the airflow through a glass wool scrubber, which quantitatively destroyed (>99%) the molecular halogens. For the I_2 measurements, an apparent interference caused higher backgrounds when measuring in the snowpack interstitial air; therefore, only background measurements made above the snowpack were used. This uncertainty in the background is accounted for in the mole ratio uncertainties shown. In 2014, SDs of background signals resulted in 3σ limits of detection (LODs) for Br_2 ranging from 1.5 to 3.9 ppt and for I_2 ranging from 0.2 to 0.5 ppt. The method uncertainty in the I_2 and Br_2 mole ratios was (–33%/+35% + LOD) and (–19%/+21% + LOD), respectively. The 2014 and 2016 CIMS molecular halogen data are available through the NSF Arctic Data Center.

Interstitial snowpack air and depth profile sampling was conducted using a 380-cm-long, 1.3-cm ID FEP-Teflon line heated to 25 °C, which was attached directly to the CIMS sampling inlet. Estimated line losses, based on laboratory and field testing of the lines with permeation devices, were accounted for in the method uncertainties (*SI Methods*). To prevent heterogeneous recycling (65), the line was rinsed with Milli-Q water and dried with N_2 before each experiment. A custom machined PTFE snow probe (Fig. S5) was used to prevent snow from entering the sampling line. A custom-built 61 × 61 cm Acrylite OP-4 cover (80% transmittance at 300 nm and ∼92% at 395 nm) with a 7.6-cm aluminum lip was pressed into the snow surface to prevent ambient air from being pulled directly into the snowpack and mixing with the interstitial air being sampled below (Fig. S6). Although dilution of the snowpack interstitial air by ambient air will occur to some extent, the O_3 mole ratios measured during in-snowpack experiments were consistently much lower than those observed in the air above the snowpack and agreed with previous snowpack O_3 observations (66, 67), suggesting that the mixing of ambient air into the snowpack was minimal. Any mixing of air within the snowpack due to high sampling rates would be expected to lessen the gradients shown in Fig. 3 and Fig. S1. O_3 was measured using a 2B Technologies model 205 dual-beam O_3 monitor. Artificial light was supplied by six Q-Lab UVA-340 halogen light bulbs (68) housed in a custom-built heated and insulated fixture. The light exited the fixture through a sheet of Acrylite OP-4, which insulated the light bulbs from the cold environment. The lamp housing was suspended ∼10 cm above the snow cover (Fig. S6).

Snow samples were collected ∼50 m upwind (north to northeast) of the CIMS sampling site on the BEO using a polypropylene scoop, which was rinsed with ACS-grade methanol and air dried before sampling. Samples were stored frozen (–10 °C to –40 °C) in polyethylene bags until the day of analysis. An Agilent Technologies 1200 series ion chromatograph (IC) was paired with a Thermo Scientific Element XR inductively coupled plasma mass spectrometer (ICP-MS) for quantitation of I^- in snowmelt samples. The 3σ limits of detection for iodide (I^-) were 1.2–5.2 pM. Na^+, Cl^-, and Br^- were determined using Dionex ICS-1100 and ICS-2100 chromatography systems, respectively, with conductivity detectors. Additional IC and IC-ICP-MS analysis details can be found in *SI Methods*. I^- enrichment factors relative to seawater were calculated using the ratio of I^- to Na^+ in seawater off the coast of Iceland ($I^-/Na^+ = 6.2 \times 10^{-8}$) (69). Br^- enrichment factors were calculated based on seawater off the coast of Utqiaġvik ($Br^-/Na^+ = 2.0 \times 10^{-3}$) (49).

Boundary layer modeling was constrained using Br_2, HOBr, Cl_2, and radiation data from a 7-h period on March 11, 2012, during the Bromine Ozone and Mercury Experiment (BROMEX) (Fig. S4) (7, 8, 22, 70). The zero-dimensional model is a series of explicit gas-phase reactions (Tables S1 and S2) and ref. 13. Initial gas-phase mole ratios (for species not constrained to observations) and photolysis rate constants are shown in Tables S1 and S3. Photolysis rate constants were obtained using the National Center for Atmospheric Research Tropospheric and UV (TUV) Radiation Model (https://www2.acom.ucar.edu/modeling/tropospheric-ultraviolet-and-visible-tuv-radiation-model) and scaled to radiation measurements from the NOAA Global Monitoring Division Earth Systems Research Laboratory (https://esrl.noaa.gov/gmd/).

ACKNOWLEDGMENTS. We thank the staff of the Jonathan Amy Facility for Chemical Instrumentation at Purdue University for building the snow cover and light fixture. Solar radiation data were acquired by and obtained from the National Oceanic & Atmospheric Administration, Earth System Research Laboratory, Global Monitoring Division Solar Radiation group. Photolysis rates were obtained using the TUV model from the National Center for Atmospheric Research, Atmospheric Chemistry Division, Chemical Processes and Regional Modeling group. We also thank Ukpeaġvik Iñupiat Corporation Science and CH2MHILL Polar Services for field logistical support and T. Miller (Birck Nanotechnology Center) for nano-pure water for chromatography. P. Burroff-Murr (Purdue University) consulted on the graphic design of Fig. 1. Financial support was provided by NSF Division of Polar Programs ARC-1107695,

PLR-1417906, and PLR-1417668. For the 2012 measurements, K.A.P. was supported by NSF Postdoctoral Fellowship in Polar Regions Research ARC-1103423. IC-ICPMS analyses were performed at the Environmental Molecular Sciences Laboratory, a national scientific user facility located at the Pacific Northwest National Laboratory (PNNL) and sponsored by the Office of Biological and Environmental Research of the US Department of Energy (DOE). PNNL is operated for the DOE by Battelle Memorial Institute under Contract DE-AC06-76RL0 1830.

1. Barrie LA, Bottenheim JW, Schnell RC, Crutzen PJ, Rasmussen RA (1988) Ozone destruction and photochemical reactions at polar sunrise in the lower Arctic atmosphere. *Nature* 334:138–141.
2. Oltmans SJ (1981) Surface ozone measurements in clean air. *J Geophys Res* 86:1174–1180.
3. Sturges WT, Barrie LA (1988) Chlorine, bromine, and iodine in Arctic aerosols. *Atmos Environ* 22:1179–1194.
4. Barrie LA, den Hartog G, Bottenheim JW, Landsberger S (1989) Anthroprogenic aerosols and gases in the lower troposphere at Alert Canada in April 1986. *J Atmos Chem* 9:101–127.
5. Liao J, et al. (2012) Observations of inorganic bromine (HOBr, BrO, and Br2) speciation at Barrow, Alaska, in spring 2009. *J Geophys Res* 117:D00R16.
6. Hausmann M, Platt U (1994) Spectroscopic measurement of bromine oxide and ozone in the high Arctic during Polar Sunrise Experiment 1992. *J Geophys Res* 99:25399–25413.
7. Pratt KA, et al. (2013) Photochemical production of molecular bromine in Arctic surface snowpacks. *Nat Geosci* 6:351–356.
8. Peterson PK, et al. (2015) Dependence of the vertical distribution of bromine monoxide in the lower troposphere on meteorological factors such as wind speed and stability. *Atmos Chem Phys* 15:2119–2137.
9. Foster KL, et al. (2001) The role of Br2 and BrCl in surface ozone destruction at polar sunrise. *Science* 291:471–474.
10. Hönninger G, Platt U (2002) Observations of BrO and its vertical distribution during surface ozone depletion at Alert. *Atmos Environ* 36:2481–2489.
11. Simpson WR, et al. (2007) Halogens and their role in polar boundary-layer ozone depletion. *Atmos Chem Phys* 7:4375–4418.
12. Wennberg PO (1999) Bromine explosion. *Nature* 397:299–301.
13. Thompson CR, et al. (2015) Interactions of bromine, chlorine, and iodine photochemistry during ozone depletions in Barrow, Alaska. *Atmos Chem Phys* 15:9651–9679.
14. Toyota K, McConnell JC, Staebler RM, Dastoor AP (2014) Air–snowpack exchange of bromine, ozone and mercury in the springtime Arctic simulated by the 1-D model PHANTAS – Part 1: In-snow bromine activation and its impact on ozone. *Atmos Chem Phys* 14:4101–4133.
15. Thomas JL, et al. (2011) Modeling chemistry in and above snow at Summit, Greenland – Part 1: Model description and results. *Atmos Chem Phys* 11:4899–4914.
16. Saiz-Lopez A, et al. (2007) Boundary layer halogens in coastal Antarctica. *Science* 317: 348–351.
17. Saiz-Lopez A, et al. (2014) Iodine chemistry in the troposphere and its effect on ozone. *Atmos Chem Phys* 14:13119–13143.
18. Calvert JG, Lindberg SE (2004) Potential influence of iodine-containing compounds on the chemistry of the troposphere in the polar spring. I. Ozone depletion. *Atmos Environ* 38:5087–5104.
19. Rowley DM, Bloss WJ, Cox RA, Jones RL (2001) Kinetics and products of the IO + BrO reaction. *J Phys Chem A* 105:7855–7864.
20. Sander SP, et al. (2006) Chemical kinetics and photochemical data for use in atmospheric studies (Jet Propulsion Lab, NASA, Pasadena, CA), Evaluation no. 15.
21. Liao J, et al. (2014) High levels of molecular chlorine in the Arctic atmosphere. *Nat Geosci* 7:91–94.
22. Custard KD, Pratt KA, Wang S, Shepson PB (2016) Constraints on Arctic atmospheric chlorine production through measurements and simulations of Cl 2 and ClO. *Environ Sci Technol* 50:acs.est.6b03909.
23. Zielcke J (2015) Observations of reactive bromine, iodine and chlorine species in the Arctic and Antarctic with differential optical absorption spectroscopy. PhD dissertation (Ruperto-Carola University, Heidelberg), 10.1017/CBO9781107415324.004.
24. Sipilä M, et al. (2016) Molecular-scale evidence of aerosol particle formation via sequential addition of HIO3. *Nature* 537:532–534.
25. Saiz-Lopez A, et al. (2012) Atmospheric chemistry of iodine. *Chem Rev* 112:1773–1804.
26. Atkinson HM, et al. (2012) Iodine emissions from the sea ice of the Weddell Sea. *Atmos Chem Phys* 12:11229–11244.
27. Saiz-Lopez A, Chance K, Liu X, Kurosu TP, Sander SP (2007) First observations of iodine oxide from space. *Geophys Res Lett* 34:L12812.
28. Frieß U, Deutschmann T, Gilfedder BS, Weller R, Platt U (2010) Iodine monoxide in the Antarctic snowpack. *Atmos Chem Phys* 10:2439–2456.
29. Mahajan AS, et al. (2010) Evidence of reactive iodine chemistry in the Arctic boundary layer. *J Geophys Res* 115:D20303.
30. Allan JD, et al. (2014) Iodine observed in new particle formation events in the Arctic atmosphere during ACCACIA. *Atmos Chem Phys* 14:28949–28972.
31. Saiz-Lopez A, Plane JMC (2004) Novel iodine chemistry in the marine boundary layer. *Geophys Res Lett* 31:L04112.
32. Mcfiggans G, et al. (2004) Direct evidence for coastal iodine particles from Laminaria macroalgae – linkage to emissions of molecular iodine. *Atmos Chem Phys Atmos Chem Phys* 4:701–713.
33. Saiz-Lopez A, et al. (2006) Modelling molecular iodine emissions in a coastal marine environment: The link to new particle formation. *Atmos Chem Phys* 6:883–895.
34. Saiz-Lopez A, Blaszczak-Boxe CS, Carpenter LJ (2015) A mechanism for biologically-induced iodine emissions from sea-ice. *Atmos Chem Phys* 15:10257–10297.
35. Saiz-Lopez A, Blaszczak-Boxe CS (2016) The polar iodine paradox. *Atmos Environ* 145:72–73.
36. Custard KD, Raso ARW, Shepson PB, Staebler RM, Pratt KA (2017) Production and release of molecular bromine and chlorine from the Arctic coastal snowpack. *ACS Earth Sp Chem* 1: 10.1021/acsearthspacechem.7b00014.
37. Wren SN, Donaldson DJ, Abbatt JPD (2013) Photochemical chlorine and bromine activation from artificial saline snow. *Atmos Chem Phys* 13:9789–9800.
38. Abbatt J, et al. (2010) Release of gas-phase halogens by photolytic generation of OH in frozen halide-nitrate solutions: An active halogen formation mechanism? *J Phys Chem A* 114:6527–6533.
39. Adams JW, Holmes NS, Crowley JN (2002) Uptake and reaction of HOBr on frozen and dry NaCl/NaBr surfaces between 253 and 233 K. *Atmos Chem Phys* 2:79–91.
40. Huff AK, Abbatt JPD (2002) Kinetics and product yields in the heterogeneous reactions of HOBr with ice surfaces containing NaBr and NaCl. *J Phys Chem A* 106:5279–5287.
41. Kirchner U, Benter T, Schindler RN (1997) Experimental verification of gas phase bromine enrichment in reaction of HOBr with sea salt doped ice surfaces. *Berichte der Bunsengesellschaft für Phys Chemie* 977:975–977.
42. Oldridge NW, Abbatt JPD (2011) Formation of gas-phase bromine from interaction of ozone with frozen and liquid NaCl/NaBr solutions: Quantitative separation of surficial chemistry from bulk-phase reaction. *J Phys Chem A* 115:2590–2598.
43. Oum KW, Lakin MJ, Finlayson-Pitts BJ (1998) Bromine activation in the troposphere by the dark reaction of O_3 with seawater ice. *Geophys Res Lett* 25:3923–3926.
44. Sjostedt SJ, Abbatt JPD (2008) Release of gas-phase halogens from sodium halide substrates: Heterogeneous oxidation of frozen solutions and desiccated salts by hydroxyl radicals. *Environ Res Lett*, 10.1088/1748-9326/3/4/045007.
45. Kim K, et al. (2016) Production of molecular iodine and triiodide in the frozen solution of iodide: Implication for polar atmosphere. *Environ Sci Technol* 50:1280–1287.
46. Gálvez O, Baeza-romero MT, Sanz M, Saiz-Lopez A (2016) Photolysis of frozen iodate salts as a source of active iodine in the polar environment. *Atmos Chem Phys* 16:12703–12713.
47. Carpenter LJ, et al. (2013) Atmospheric iodine levels influenced by sea surface emissions of inorganic iodine. *Nat Geosci* 6:108–111.
48. King MD, Simpson WR (2001) Extinction of UV radiation in Arctic snow at Alert, Canada. *J Geophys Res* 106:12499–12507.
49. Simpson WR, Alvarez-aviles L, Douglas TA, Sturm M, Domine F (2005) Halogens in the coastal snow pack near Barrow, Alaska: Evidence for active bromine air-snow chemistry during springtime. *Geophys Res Lett* 32:2–5.
50. Xu W, Tenuta M, Wang F (2016) Bromide and chloride distribution across the snow-sea-ice-ocean interface: A comparative study between an Arctic coastal marine site and an experimental sea ice mesocosm. *J Geophys Res Ocean* 121:1063–1084.
51. Saiz-Lopez A, Saunders RW, Joseph DM, Ashworth SH, Plane JMC (2004) Absolute absorption cross-section and photolysis rate of I2. *Atmos Chem Phys* 4:1443–1450.
52. Bartels-Rausch T, et al. (2014) A review of air-ice chemical and physical interactions (AICI): Liquids, quasi-liquids, and solids in snow. *Atmos Chem Phys* 14:1587–1633.
53. Jacob DJ (2000) Heterogeneous chemistry and tropospheric ozone. *Atmos Environ* 34: 2131–2159.
54. Sander R (2015) Compilation of Henry's law constants (version 4.0) for water as solvent. *Atmos Chem Phys* 15:4399–4981.
55. France JL, et al. (2012) Hydroxyl radical and NOx production rates, black carbon concentrations and light-absorbing impurities in snow from field measurements of light penetration and nadir reflectivity of onshore and offshore coastal Alaskan snow. *J Geophys Res*, 10.1029/2011JD016639.
56. Simpson WR, Brown SS, Saiz-Lopez A, Thornton JA, Glasow Rv (2015) Tropospheric halogen chemistry: Sources, cycling, and impacts. *Chem Rev* 115:4035–4062.
57. Holmes NS, Adams JW, Crowley JN (2001) Uptake and reaction of HOI and IONO on frozen and dry NaCl/NaBr surfaces and H2SO4. *Phys Chem Chem Phys* 9:1679–1687.
58. Troy RC, Kelley MD, Nagy JC, Margerum DW (1991) Non-metal redox kinetics: Iodine monobromide reaction with iodide ion and the hydrolysis of IBr. *Inorg Chem* 30:4838–4845.
59. Beckwith RC, Wang TX, Margerum DW (1996) Equilibrium and kinetics of bromine hydrolysis. *Inorg Chem* 35:995–1000.
60. Halfacre JW, et al. (2014) Temporal and spatial characteristics of ozone depletion events from measurements in the Arctic. *Atmos Chem Phys* 14:4875–4894.
61. Sommariva R, Bloss WJ, von Glasow R (2012) Uncertainties in gas-phase atmospheric iodine chemistry. *Atmos Environ* 57:219–232.
62. Domine F, Bock J, Voisin D, Donaldson DJ (2013) Can we model snow photochemistry? Problems with the current approaches. *J Phys Chem A* 117:4733–4749.
63. Saiz-Lopez A, et al. (2012) Estimating the climate significance of halogen-driven ozone loss in the tropical marine troposphere. *Atmos Chem Phys* 12:3939–3949.
64. Liao J, et al. (2011) A comparison of Arctic BrO measurements by chemical ionization mass spectrometry and long path-differential optical absorption spectroscopy. *J Geophys Res* 116:D00R02.
65. Neuman JA, et al. (2010) Bromine measurements in ozone depleted air over the Arctic Ocean. *Atmos Chem Phys* 10:6503–6514.
66. Peterson MC, Honrath RE (2001) Observations of rapid photochemical destruction of ozone in snowpack interstitial air. *Geophys Res Lett* 28:511–514.
67. Van Dam B, et al. (2015) Dynamics of ozone and nitrogen oxides at Summit, Greenland: I. Multi-year observations in the snowpack. *Atmos Environ* 123:268–284.
68. Q-Lab Corporation (2011) Spectral power distribution for QUV with UVA-340 fluorescent lamps. Technical Bulletin LU-8052. Available at www.q-lab.com/products/lamps-optical-filters/lamps-and-optical-filters. Accessed December 3, 2014.
69. Waite TJ, Truesdale VW, Olafsson J (2006) The distribution of dissolved inorganic iodine in the seas around Iceland. *Mar Chem* 101:54–67.
70. Nghiem SV, et al. (2013) Studying bromine, ozone, and mercury chemistry in the Arctic. *Eos (Wash DC)* 94:2012–2013.